

Modification of the dye-sensitized solar cells photoanode by changing the immersion time and dye concentration

Ewelina Krawczak^{1*} , Agata Zdyb¹ 

¹ Department of Renewable Energy Engineering, Faculty of Environmental Engineering, Lublin University of Technology, Nadbystrzycka 40B, 20-618 Lublin, Poland

* Corresponding author's e-mail: krawczak@pollub.pl

ABSTRACT

Dye-sensitized solar cells (DSSCs), together with organic and perovskite cells, represent the third generation of photovoltaic solar cells. DSSCs are characterized by reasonable fabrication costs, low weight, and relatively high conversion efficiency in diffuse radiation with good absorption regardless of the angle of incidence of the sun's rays. However, there is still a great need to improve the working parameters of dye-sensitized solar cells. The dye sensitizer is one of the crucial components that strongly affects the performance of DSSC by extending the range of light absorption. The objective of this study is to report the influence of photoanode immersion time on the working parameters of catechol-based dye-sensitized cells. According to theoretical investigation, catechol is a metal-free organic dye that can be implemented in DSSC. The DSSC assemblies were carefully fabricated in a sandwich way with the use of TiO₂-based photoanodes, Pt counter electrodes, and iodide/triiodide electrolytes. A relationship between photoanode sensitization time and DSSC efficiency was established and then optimized. The optical and electrical measurements were carried out; the dye/TiO₂ complexes were characterized by UV–Vis spectrophotometric analysis, while the prepared cells were tested using a solar light simulator under standard test conditions (STC). The role of the back reflector layer made of BaSO₄ on conversion efficiency was also investigated.

Keywords: dye-sensitized solar cells, photovoltaic, dyes, catechol.

INTRODUCTION

Nowadays, fossil fuels represent the primary source of global energy production, accounting for about 82% [1]. The significant development of industry and society, unsustainable energy usage, and thus the increase in energy demand, have led to concerns about the depletion of these natural resources [2]. It is possible that a shortage of the main fossil fuels, such as coal, natural gas, and petroleum, may occur in the near future. Natural gas and oil consumption is expected to remain at about the same level as today. However, the use of coal is projected to decline by 2050 [3].

There is a significant interdependence between global society and climate, with climate change adaptation and sustainable development demonstrating a close correlation. The use of renewable energy sources (RESs), which means

energy-related greenhouse gasses (GHGs) emission reduction and energy transition, has become a matter of global concern. Net Zero Emissions by 2050 is a global scenario that depicts the pathway to achieve net zero emissions of greenhouse gases by 2050. The main goal is to limit the temperature rise to 1.5 °C above pre-industrial levels, which is also consistent with the Paris Agreement [Annex to the Proposal for a Regulation of the European Parliament and of the Council amending Regulation (EU) 2018/842 on binding annual greenhouse gas emission reductions by Member States from 2021 to 2030 contributing to climate action to meet commitments under the Paris Agreement, 2021]. Among all renewable energy sources, solar energy is highly promising. According to Energy Transition Outlook 2023 [5], it is predicted that solar capacity, including on-grid and off-grid photovoltaic (PV) systems, will rise from 1200 GW to

9100 GW in the next 10 years, and to 33000 GW in 2050. Photovoltaics is an attractive technology that directly converts sunlight into the most usable energy form – electricity via the photoelectric effect, which is the reason why there is a constant research interest in this field. Photovoltaic technology is categorized into three generations. The first one is dedicated to silicon-based solar cells, with an efficiency of 26.7% obtained for mono-crystalline lab cells [6, 7]. Various research studies are concerned with the performance of photovoltaic installations at different latitudes [8–11]. The second generation of solar cells is based on thin-film technologies, such as copper-indium-gallium diselenide (CIGS), copper-indium diselenide (CIS), cadmium telluride (CdTe) or amorphous silicon (aSi). The CdTe laboratory module achieved an efficiency of 19.5%, while CIGS module - 19.2% [6]. Due to high efficiencies, the modules belonging to the first and second generation are fully commercialized and have been used for years both in small on-grid or hybrid installations as well as in large-scale plants [12]. However, the performance of traditional silicon and thin film technologies varies depending on location therefore the investigations carried out at various latitudes are of high importance [8, 11, 13, 14], especially in the context of increased interest in solar energy.

The third generation of solar cells includes emerging photovoltaic technologies that can be considered as replacements for the 1st and 2nd generation. What is even more, they can reduce the cost of manufacturing solar cells by using inexpensive and environmentally friendly production processes [15]. The first representative of this generation was the dye-sensitized solar cells discovered by O'Regan and Grätzel in 1991 [16], which were an innovative approach to a photocatalytic solar cell. Others are perovskites [17] and organic solar cells [18] with the efficiency of modules equal to 26.1% [19] and 14.5% [20], respectively.

Dye-sensitized solar cells are photoelectrochemical devices consisting of a photoanode (PA), counter electrode (CE), electrolyte, and sensitizer. Both electrodes are covered with transparent conductive oxides (TCO), mainly with indium tin oxide (ITO) and fluorine tin oxide (FTO) due to their electrical, chemical, and thermal properties. A mesoporous titanium dioxide (TiO_2) layer is deposited on the top PA, while a platinum catalyst layer is deposited on the CE. The device is filled with an electrolyte solution, which is typically a liquid but can also exist in a quasi-solid or solid state. The

sensitizer, which is the key component, is absorbed onto the TiO_2 surface for optimum light absorption and efficient charge transfer, Natural and organic sensitizers have the potential to be used in dye-sensitized solar cells [21, 22]. However, they must meet certain requirements, such as absorption of the solar light in a wide range, suitable chemical structure with the anchoring group, or appropriate energy levels [23]. The selection of sensitizer plays a crucial role in cell stability, working parameters, and therefore overall cell efficiency. According to the findings of Roland et al. [24], the dyes can be categorized into two distinct groups: metal-complex and metal-free organic dyes. However, it should be noted that among these photosensitizers are those that are either natural or synthetic-based [25]. The catechol dye belongs to a metal-free class of sensitizers, which is important considering the environmental impact of dye cell technology and the life cycle assessment of prospective applications. The structure of the catechol unit is also present in numerous other dyes with complex molecules, metal-based compounds among them [26], where it serves as an anchoring group ensuring a strong chelating bond with the surface of titanium dioxide nanoparticles. The advantages of catechol's role in adsorption include high stability of the dye on the TiO_2 surface [27] and enhancement of electric charge transfer from the dye to a semiconductor, which is a critical step in the work cycle of DSSC [28].

The presented research on catechol as a sensitizer in DSSC is based on previous experience with different practical factors influencing the performance of dye cells [29]. This investigation established the correlation between photovoltaic parameters of the photocells and the time, in which the photoanode covered with TiO_2 nanoparticles soaks the solution of the sensitizer as well as the concentration of the solution. Moreover, the effect of the reflection of light from the additional layer introduced in the structure of the tested cells was assessed quantitatively.

MATERIALS AND METHODS

The glass electrodes covered with a fluorine tin oxide (FTO) layer and counter electrodes with platinum black coverage were purchased from the Greatcell Solar company. The FTO substrates were characterized by a sheet resistance equal to $7 \Omega/\text{sq}$ and a transmittance of 82%. All chemicals

used in the experiments were commercially available and were utilized without additional purification processes. After chemical and ultrasonic cleaning with the use of detergent, acetone, and absolute ethanol, the FTO electrodes were used as substrates for photoanodes. The titanium dioxide paste was prepared according to the procedure presented in [30] with the use of Degussa TiO₂ nanoparticles PN25. Then, the TiO₂ paste was deposited uniformly onto FTO in a rectangular shape with an area of 0.8 cm² by the use of the standard doctor-blade technique [31]. The deposited layers were sintered at 450 °C in a Gestigkeit PZ 28-3T high-temperature hot plate with a lid, controlled by PR 5-3T PID Programme Regulator. The layers cooled down naturally inside the hot plate. Afterward, the as-prepared electrodes

with the mesoporous TiO₂ layer were immersed in a solution of catechol (CAT) dye and absolute ethanol. The molecular structure of catechol dye is depicted in Figure 1a. The research was carried out with three dye concentrations (0.25 mM, 1.0 mM, and 2.0 mM) and various immersion times. The immersion process was conducted without access to light. The photoanodes after sensitization are presented in Figure 1b. In order to achieve the greatest solubility, catechol solutions were ultrasonically mixed before use. After sensitization, the electrodes were rinsed with absolute ethanol to eliminate nonadsorbed molecules of the dye. The Surlyn separator (DyeSol) was used to encapsulate the sandwich-structure DSSC device. The scheme of the dye-sensitized solar cell is presented in Figure 2.

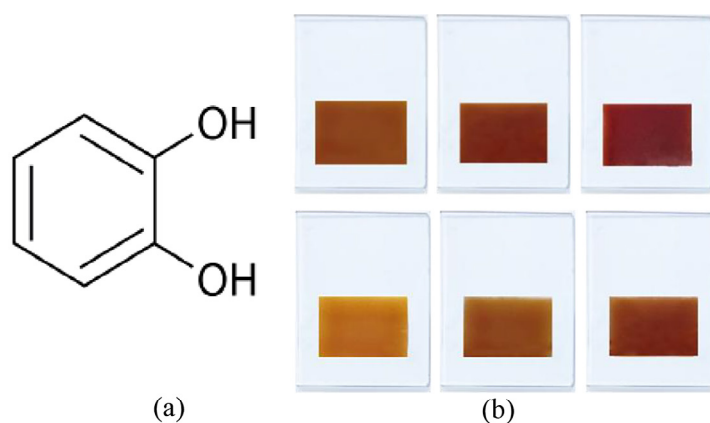


Figure 1. (a) The molecular structure of catechol molecule. (b) The working electrodes were sensitized for: (from left) 10 min, 30 min, 1 h, 2 h, 4 h, and 24 h in catechol solution

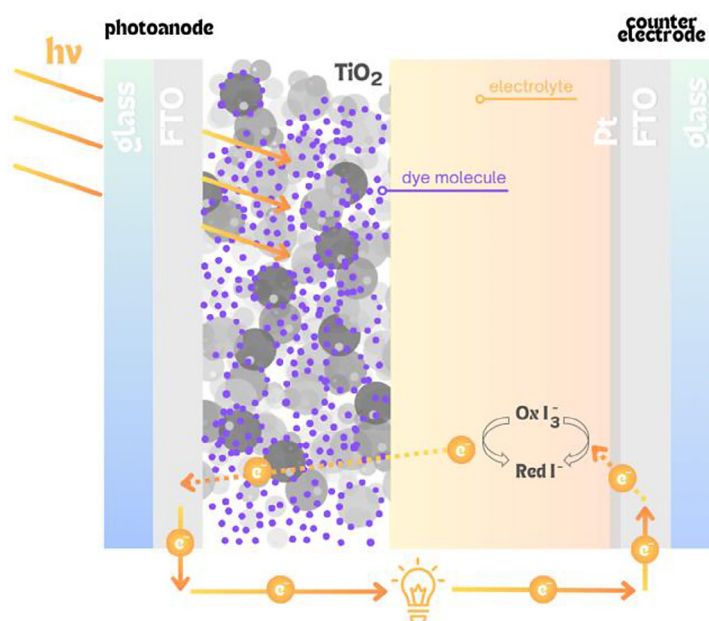


Figure 2. Scheme of dye-sensitized solar cell

After the encapsulation process, the electrolyte containing a redox (I^+/I_3^-) mediator (Greatcell Solar) was injected between the photoanode and cathode by the drilled hole in the counter electrode. The working parameters of the prepared DSSC were measured by the use of a solar simulator (Abet Technologies SUN 300, class AAA) in standard test conditions (STC), namely $G = 1000 \text{ W/m}^2$, $T = 25 \text{ }^\circ\text{C}$, and $AM = 1.5$. The I-V curves were determined by the Keithley 2440 source meter, which cooperates with the solar simulator. The efficiencies of the cells were calculated by the use of Matlab software, according to Equation 1 [32].

$$\eta = \frac{I_{SC} \cdot V_{OC} \cdot FF}{P_{in}} [-] \quad (1)$$

where: I_{SC} is short circuit current [A], V_{OC} is open-circuit voltage [V], FF is fill factor [-], which can be determined by Equation 2, and P_{in} is incident light power [W] evaluated by Equation 3.

$$FF = \frac{P_{MAX}}{I_{SC} \cdot V_{OC}} [-] \quad (2)$$

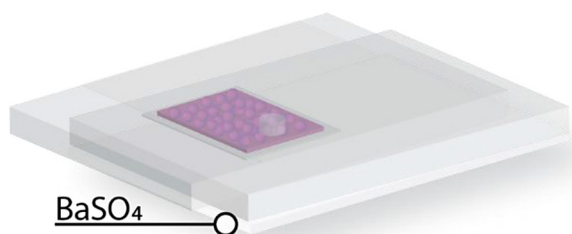


Figure 3. Implementation of BaSO₄ reflective layer in DSSC

$$P_{in} = G \cdot A \quad (3)$$

where: P_{MAX} is maximum output power [W], G is irradiation [W/m^2], and A is the active area of the cell [m^2].

The measurements were carried out with or without an additional, reflective layer made of barium sulfate (BaSO₄). The implementation of BaSO₄ is depicted in Figure 3. The absorbance spectra were performed by Thermo Scientific Evolution 220 UV-visible spectrophotometer. The measurements were carried out in the light wavelength range of 200–1100 nm, with an accuracy of 1 nm, at room temperature (RT).

RESULTS AND DISCUSSION

Spectrophotometric characterization

The catechol solution exhibits absorbance in a narrow band in the ultraviolet region of the spectrum with a major peak around $\lambda = 275 \text{ nm}$ (Figure 4a). Similar values were reported in the work of Wang et al. [33]. Absorbance spectra of bare titanium oxide nanoparticles and CAT/TiO₂ complex photoanodes are presented in Figure 4b. The TiO₂ photoanode is characterized by the absorption of solar radiation in a narrow range of the spectrum, namely in the ultraviolet region. After a sensitization process by immersion in the dye solution, and thus the creation CAT/TiO₂ complex, the increase in the light absorption intensity and expansion of the range were observed. The broad absorption band can be seen

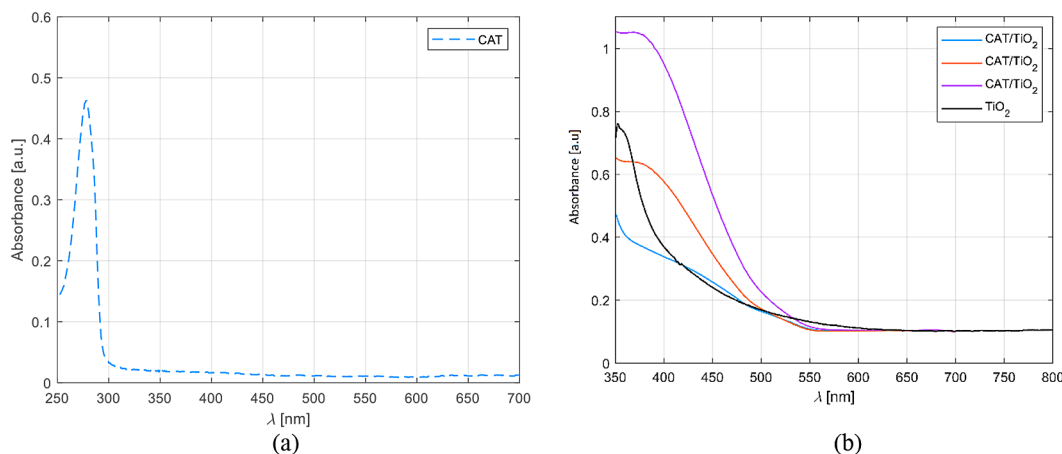


Figure 4. (a) Absorbance spectra of the catechol dye solution in absolute ethanol, (b) absorbance spectra of the CAT/TiO₂ complex for 1 min (blue line), 2 min (orange line), 3 min (violet line), and TiO₂ photoanode

in the range of 350 ÷ 550 nm, while the absorption peak was detected at 350÷390 nm.

Three sets of solar cells, each with a different concentration of dye solution, were prepared according to a described procedure in Section Materials and Methods. The immersion times were carefully selected during the research process, and accordingly, for the 0.25 mM catechol concentration were chosen: 10 minutes, 30 minutes, 1 hour, 2 hours, 4 hours, and 24 hours. The I-V measurements were carried out for freshly made DSSCs with and without the reflective layer. Working parameters of DSSCs which were obtained without a BaSO₄ layer are depicted in Table 1. The open-circuit voltage values were in the range of 45.06 mV (CAT-5)÷142.34 mV (CAT-3). The highest V_{OC} value was obtained for an immersion time of 1 h. The values of I_{SC} were in the range of 0.006÷0.12 mA, and they were noticed for CAT-4, and for CAT-1, CAT-3, respectively. The highest FF was registered for solar cells immersed in dye solution for 2 hours.

The results obtained for samples with reflective layers are depicted in Table 2. Application of the BaSO₄ reflective layers led to achieving better working parameters. For the DSSC immersed for 30 minutes, the 13% increase in V_{OC} and I_{SC} values can be observed, however, the maximum power point value increased by 41%, as did the efficiency. The best working parameters were

recorded for the CAT-3, which was immersed in catechol solution for 1 hour. The sample is characterized by an open circuit voltage of 142.34 mV, a short circuit current of 0.012 mA, a fill factor of 23.35% and an efficiency equals 0.0005%. Immersion times for the dye solutions of 1.0 mM and 2.0 mM were established as follows: 1h, 2h, 4h, and 24 hours. The results for dye-sensitized solar cells without the reflective layer, obtained by immersion in 1.0 mM catechol solution, are depicted in Table 3. At the outset, the cells were characterized by the following parameters: I_{SC} in the range of 0.003 mA (CAT-7)÷0.014 mA (CAT-9) and V_{OC} ranging between 62.08 mV (CAT-10) and 93.63 mV (CAT-9). The maximum power point values of DSSCs without reflective layer equaled to 32.77 mV (CAT-10)÷56.29 mV (CAT-9). The current values at the maximum power point for most of the fabricated cells (CAT-7, CAT-8, and CAT-10) were 0.002 mA, while for the CAT-9 cell – 0.004 mA. These cells also showed an increase in working parameters after the application of the BaSO₄ layer (Table 4) with up to 15% increase for I_{SC} values, 50% for I_{MPP}, 6% for V_{OC}, and 70% for V_{MPP}. The range for short circuit current values was 0.004 mA (CAT-7) to 0.016 mA (CAT-9), while open circuit values ranged from 65.09 mV (CAT-10) to 99.82 mV (CAT-7). The highest value of FF was obtained for both cases, with and

Table 1. Working parameters of DSSCs immersed in 0.25 mM catechol solution; without a BaSO₄ reflective layer

ID	Time	I _{SC}	V _{OC}	I _{MPP}	V _{MPP}	P _{MPP}	FF	η
		[mA]	[mV]	[mA]	[mV]	[mW]	[%]	[%]
CAT-1	10 min	0.012	136.17	0.005	75.02	0.0004	22.83 ± 0.83	(4.80 ± 0.11) · 10 ⁻⁴
CAT-2	30 min	0.009	53.14	0.003	28.17	0.0001	17.63 ± 1.19	(1.02 ± 0.03) · 10 ⁻⁴
CAT-3	1 h	0.012	142.34	0.005	84.48	0.0004	23.35 ± 1.03	(5.06 ± 0.12) · 10 ⁻⁴
CAT-4	2 h	0.006	138.45	0.003	79.71	0.0002	31.14 ± 0.60	(2.99 ± 0.08) · 10 ⁻⁴
CAT-5	4 h	0.009	45.06	0.003	23.47	0.0001	18.02 ± 1.09	(9.53 ± 0.30) · 10 ⁻⁵
CAT-6	24 h	0.007	100.54	0.004	51.64	0.0002	31.01 ± 0.83	(2.82 ± 0.07) · 10 ⁻⁴

Table 2. Working parameters of DSSCs immersed in 0.25 mM catechol solution; with a BaSO₄ reflective layer

ID	Time	I _{SC}	V _{OC}	I _{MPP}	V _{MPP}	P _{MPP}	FF	η
		[mA]	[mV]	[mA]	[mV]	[mW]	[%]	[%]
CAT-1	10 min	0.013	140.18	0.009	51.58	0.0005	26.90 ± 0.34	(6.06 ± 0.14) · 10 ⁻⁴
CAT-2	30 min	0.010	59.89	0.004	28.17	0.0001	19.64 ± 1.05	(1.44 ± 0.04) · 10 ⁻⁴
CAT-3	1 h	0.012	148.51	0.010	51.63	0.0005	28.29 ± 0.43	(6.43 ± 0.15) · 10 ⁻⁴
CAT-4	2 h	0.006	146.87	0.003	84.38	0.0003	31.23 ± 0.62	(3.68 ± 0.09) · 10 ⁻⁴
CAT-5	4 h	0.011	46.72	0.004	23.47	0.0001	18.90 ± 0.96	(1.19 ± 0.04) · 10 ⁻⁴
CAT-6	24 h	0.011	109.59	0.004	58.79	0.0003	21.22 ± 0.83	(3.27 ± 0.08) · 10 ⁻⁴

Table 3. Working parameters of DSSCs immersed in 1.0 mM catechol solution; without a BaSO₄ reflective layer

ID	Time	I_{SC}	V_{OC}	I_{MPP}	V_{MPP}	P_{MPP}	FF	η
		[mA]	[mV]	[mA]	[mV]	[mW]	[%]	[%]
CAT-7	1 h	0.003	93.63	0.002	51.53	0.0001	27.91 ± 0.87	(1.11 ± 0.04) · 10 ⁻⁴
CAT-8	2 h	0.005	78.68	0.002	42.25	0.0001	25.44 ± 0.64	(1.22 ± 0.04) · 10 ⁻⁴
CAT-9	4 h	0.014	87.89	0.004	56.29	0.0002	20.55 ± 0.83	(3.09 ± 0.08) · 10 ⁻⁴
CAT-10	24 h	0.004	62.08	0.002	32.77	0.0001	24.57 ± 0.91	(8.20 ± 0.30) · 10 ⁻⁵

Table 4. Working parameters of DSSCs immersed in 1.0 mM catechol solution; with a BaSO₄ reflective layer

ID	Time	I_{SC}	V_{OC}	I_{MPP}	V_{MPP}	P_{MPP}	FF	η
		[mA]	[mV]	[mA]	[mV]	[mW]	[%]	[%]
CAT-7	1 h	0.004	99.82	0.002	56.23	0.0001	27.97 ± 0.71	(1.41 ± 0.04) · 10 ⁻⁴
CAT-8	2 h	0.006	80.10	0.003	42.29	0.0001	25.30 ± 0.60	(1.49 ± 0.04) · 10 ⁻⁴
CAT-9	4 h	0.016	81.68	0.008	32.89	0.0003	19.67 ± 0.69	(3.18 ± 0.09) · 10 ⁻⁴
CAT -10	24 h	0.005	65.09	0.003	32.79	0.0001	24.85 ± 0.74	(1.03 ± 0.03) · 10 ⁻⁴

Table 5. Working parameters of DSSCs immersed in 1.0 mM catechol solution; without a BaSO₄ reflective layer

ID	Time	I_{SC}	V_{OC}	I_{MPP}	V_{MPP}	P_{MPP}	FF	η
		[mA]	[mV]	[mA]	[mV]	[mW]	[%]	[%]
CAT-11	1 h	0.003	69.14	0.001	37.43	0.00005	25.88 ± 1.03	(5.83 ± 0.23) · 10 ⁻⁵
CAT-12	2 h	0.007	68.00	0.003	37.65	0.0001	27.56 ± 1.08	(1.54 ± 0.05) · 10 ⁻⁴
CAT-13	4 h	0.014	94.73	0.006	46.90	0.0003	19.81 ± 0.34	(4.35 ± 0.13) · 10 ⁻⁴
CAT -14	24 h	0.015	67.02	0.008	28.13	0.0002	22.20 ± 1.08	(2.84 ± 0.08) · 10 ⁻⁴

without a reflective layer, for samples immersed for 1 hour. However, the highest efficiency was noticed for CAT-9 with an immersion time of 4 hours, which was found to be the best for this dye concentration.

The last phase of the conducted research concerned a catechol dye solution of 2.0 mM concentration, the results of which are shown in Table 5 and Table 6. The dye-sensitized solar cells without a reflective layer were characterized with V_{OC} in the range of 67.02 mV (CAT-14) ÷ 94.73 mV (CAT-13), the values of I_{SC} between 0.003 mA (CAT-11) and 0.015 mA (CAT-14). After the application of the reflective layer, a positive change can be observed in some of the working

parameters, such as I_{SC} , I_{MPP} , V_{OC} , and V_{MPP} , to name but a few. The value of the short-circuit current and open circuit voltage of the cell CAT-11 increased by 18% and 6%, respectively. The FF values for the examined dye cells fell within the ranges 19.81÷27.56% (without BaSO₄), and 21.31÷31.78% (with BaSO₄). The further increase in immersion time does not lead to enhancements in working parameters.

Taking into consideration three sets of prepared dye-sensitized solar cells, the best working parameters were obtained for CAT-3 samples which are characterized by a 1-hour immersion time and a 0.25 mM concentration of dye solution. The boxplot of the examined efficiency values for

Table 6. Working parameters of DSSCs immersed in 1.0 mM catechol solution; with a BaSO₄ reflective layer

ID	Time	I_{SC}	V_{OC}	I_{MPP}	V_{MPP}	P_{MPP}	FF	η
		[mA]	[mV]	[mA]	[mV]	[mW]	[%]	[%]
CAT-11	1 h	0.003	73.63	0.002	37.43	0.0001	25.75 ± 0.88	(7.31 ± 0.27) · 10 ⁻⁵
CAT-12	2 h	0.007	70.58	0.004	42.33	0.0001	31.78 ± 1.32	(1.86 ± 0.05) · 10 ⁻⁴
CAT-13	4 h	0.013	87.24	0.005	46.91	0.0002	21.31 ± 1.06	(4.11 ± 0.12) · 10 ⁻⁴
CAT -14	24 h	0.016	61.86	0.008	28.12	0.0002	23.22 ± 1.11	(2.82 ± 0.08) · 10 ⁻⁴

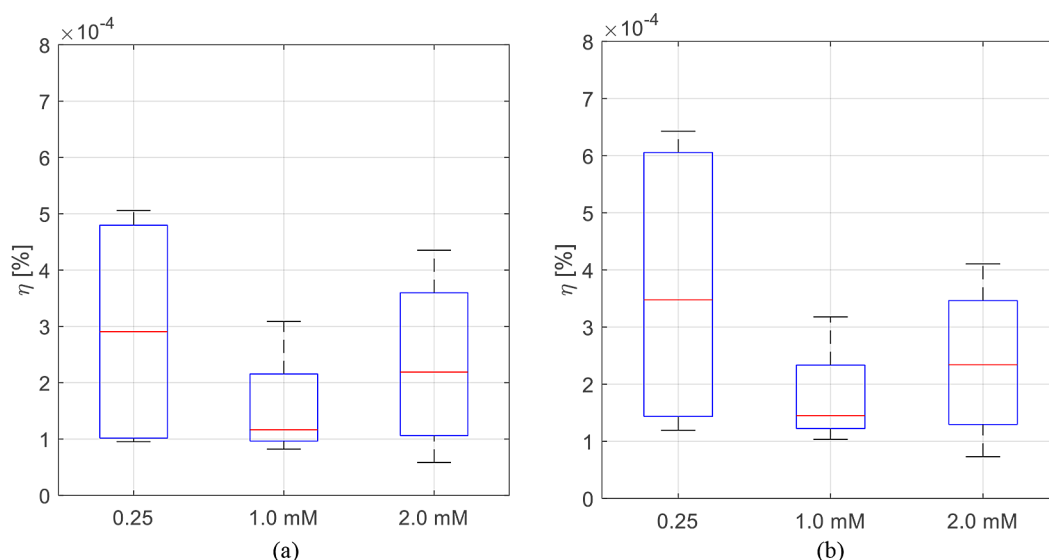


Figure 5. The efficiency of prepared cells in accordance with various dye solution concentrations (0.25 mM, 1.0 mM, and 2.0 mM) obtained: (a) without BaSO₄ layer, (b) with BaSO₄ layer

the samples prepared without and with a reflective layer is presented in Figure 5a and Figure 5b. The interquartile ranges are slightly higher for the samples with BaSO₄ layer which is correlated with the high reflectance of BaSO₄ layer, and thus higher working parameters of the cells. The median values of efficiency for the solar cells without the reflective layers were 0.00029%, 0.0001%, and 0.0002% for dye solution of 0.25 mM, 1.0 mM, and 2.0 mM, respectively. Application of the reflective layer led to median values equal to 0.00035% (0.25 mM), 0.0001% (1.0 mM), and 0.0002% (2.0 mM).

Figure 6a depicts the *I-V* characteristics of a representative dye-sensitized solar cell obtained by immersion for 2 hours in 0.25 mM dye solution obtained without reflective layer, while Figure 6b

presents the curve with BaSO₄ layer. Due to the occurrence of a local maximum in the measured data at the beginning of the current-voltage characteristic curve (at *V* = 0), in order to determine the most accurate value of the short-circuit current *I*_{sc}, the least squares method was used which is depicted as the purple line in Figure 6. The occurring maximum is related to the four-quadrant meter switching between quadrants II and I during the measurements.

In the literature, the *V*_{oc} values obtained for pyranoflavylum dyes possessing a catechol linkage unit in their structure are in the range of 252–338 mV [34] and 119–430.8 mV for other metal-free organic dyes with catechol ring in the molecular structure [35].

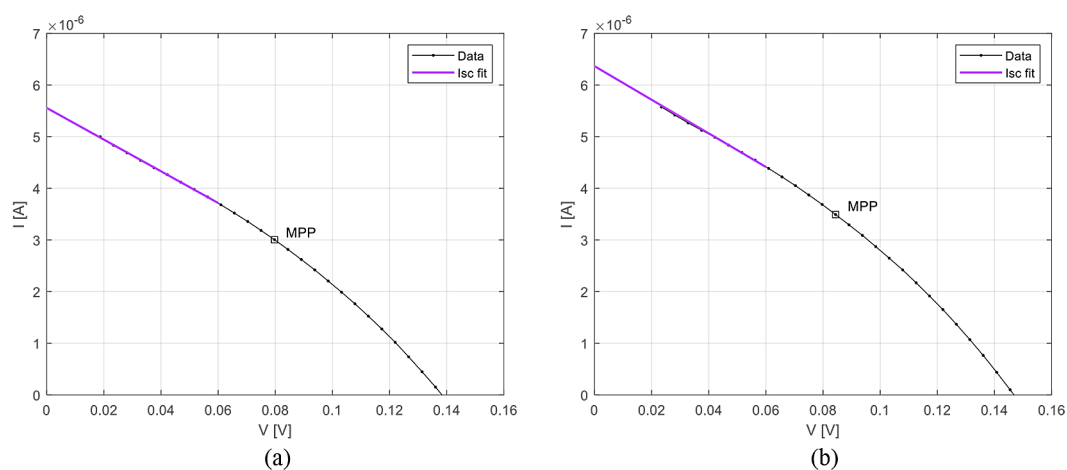


Figure 6. The *I-V* characterization of catechol dye-sensitized solar cells (2 h, 0.25 mM) obtained (a) without BaSO₄ layer, (b) with BaSO₄ layer

The observed improvement of photovoltaic parameters in the catechol-sensitized photocells with a reflective layer confirms that the introduction of this layer is justified and necessary to enhance the absorption of light. The achieved 41% increase of efficiency for 30 min dipping time and 0.25 mM concentration of catechol solution corresponds to the values of 27% improvement obtained for dye cells sensitized with phenyl fluorone [35].

CONCLUSIONS

Adsorption of catechol on the surface of TiO₂ electron transport layer results in the shift of light absorption edge to longer wavelengths compared to pristine TiO₂, thereby increasing light harvesting. Optimization of the time of immersion of the photoanode in the catechol solution and the concentration of this solution allows for improving the performance of the investigated photocells. The following experimentally determined combination of these two parameters enhances the photovoltaic parameters: 1 hour of dipping time and 0.25 mM dye concentration. An important beneficial factor is the modification of the DSSC structure by introducing a reflective layer consisting of BaSO₄, which provides an additional chance for light absorption. A comparison of the photovoltaic parameters characteristic of the catechol-sensitized cells indicates that the strategy based on adding the reflective layer leads to improved overall performance and can be used in future applications.

REFERENCES

1. Statistical Review of World Energy. 73rd edition. 2024. Energy Institute; 2024.
2. Holeček J.L., Geli H.M.E., Sawalhah M.N., Valdez R. A global assessment: Can renewable energy replace fossil fuels by 2050? *Sustainability*. 2022; 14: 4792. doi:10.3390/su14084792.
3. World Energy Outlook 2023. 2024.
4. Annex to the Proposal for a Regulation of the European Parliament and of the Council amending Regulation (EU) 2018/842 on binding annual greenhouse gas emission reductions by Member States from 2021 to 2030 contributing to climate action to meet commitments under the Paris Agreement. 2021.
5. DNV. Energy Transition Outlook 2023. Pathway to net-zero emissions. Oslo, Norway: DNV; 2024.
6. Philipps D.S., Ise F., Warmuth W., GmbH PP. Photovoltaics Report 2022. Freiburg, Germany: Fraunhofer ISE; 2023.
7. Yoshikawa K., Kawasaki H., Yoshida W., Irie T., Konishi K., Nakano K., et al. Silicon heterojunction solar cell with interdigitated back contacts for a photoconversion efficiency over 26%. *Nat Energy*. 2017; 2: 1–8. doi:10.1038/nenergy.2017.32.
8. Gulkowski S. Specific yield analysis of the rooftop pv systems located in South-Eastern Poland. *Energies*. 2022;15: 3666. doi:10.3390/en15103666.
9. Zdyb A., Szałas G. Rooftop low angle tilted photovoltaic installation under Polish climatic conditions. *J Ecol Eng*. 2021; 22: 223–233. doi:10.12911/22998993/140255.
10. Olczak P. Energy Productivity of Microinverter Photovoltaic Microinstallation: Comparison of Simulation and Measured Results—Poland Case Study. *Energies*. 2022; 15: 7582. doi:10.3390/en15207582.
11. Krawczak E. A comparative analysis of measured and simulated data of PV rooftop installations located in Poland. *Energies*. 2023; 16: 5975. doi:10.3390/en16165975.
12. Żelazna A., Gołębiowska J., Zdyb A., Pawłowski A. A hybrid vs. on-grid photovoltaic system: Multicriteria analysis of environmental, economic, and technical aspects in life cycle perspective. *Energies*. 2020; 13: 3978. doi:10.3390/en13153978.
13. Gaglia A.G., Lykoudis S., Argiriou A.A., Balaras C.A., Dialynas E. Energy efficiency of PV panels under real outdoor conditions—An experimental assessment in Athens, Greece. *Renew Energy*. 2017; 101: 236–243. doi:10.1016/j.renene.2016.08.051.
14. Micheli D., Alessandrini S., Radu R., Casula I. Analysis of the outdoor performance and efficiency of two grid connected photovoltaic systems in northern Italy. *Energy Convers Manage*. 2014; 80: 436–445. doi:10.1016/j.enconman.2014.01.053.
15. Yıldız Y., Bilen K., Atılgan A. Experimental investigation of spin coating acceleration effect on the DSSC performance. *Mater Res Express*. 2024; 11: 035502. doi:10.1088/2053-1591/ad30ad.
16. O'Regan B., Grätzel M. A low-cost, high-efficiency solar cell based on dye-sensitized colloidal TiO₂ films. *Nature*. 1991; 353: 737–740. doi:10.1038/353737a0.
17. Sharif R., Khalid A., Ahmad S.W., Rehman A., Qutab H.G., Akhtar H.H., et al. A comprehensive review of the current progresses and material advances in perovskite solar cells. *Nanoscale Adv*. 2023; 5: 3803–3833. doi:10.1039/D3NA00319A.
18. Solak E.K., Irmak E. Advances in organic photovoltaic cells: a comprehensive review of materials, technologies, and performance. *RSC Adv*. 2023; 13: 12244–12269. doi:10.1039/D3RA01454A.

19. Cao F., Bian L., Li L. Perovskite solar cells with high-efficiency exceeding 25%: A review. *Energy Materials and Devices*. 2024; 2. doi:10.26599/EMD.2024.9370018.
20. Basu R., Gumpert F., Lohbreier J., Morin P-O., Vohra V., Liu Y., et al. Large-area organic photovoltaic modules with 14.5% certified world record efficiency. *Joule*. 2024; 8: 970–978. doi:10.1016/j.joule.2024.02.016.
21. Lee T.D., Ebong A.U. A review of thin film solar cell technologies and challenges. *Renew Sustain Energy Rev*. 2017; 70: 1286–1297. doi:10.1016/j.rser.2016.12.028.
22. Omar A., Ali M.S., Abd Rahim N. Electron transport properties analysis of titanium dioxide dye-sensitized solar cells (TiO₂-DSSCs) based natural dyes using electrochemical impedance spectroscopy concept: A review. *Sol Energy*. 2020; 207: 1088–1121. doi:10.1016/j.solener.2020.07.028.
23. Hagfeldt A., Boschloo G., Sun L., Kloo L., Pettersson H. Dye-sensitized solar cells. *Chem Rev*. 2010; 110: 6595–6663. doi:10.1021/cr900356p.
24. Roslan N., Ya'acob M.E., Radzi M.A.M., Hashimoto Y., Jamaludin D., Chen G. Dye Sensitized Solar Cell (DSSC) greenhouse shading: New insights for solar radiation manipulation. *Renewable and Sustainable Energy Reviews*. 2018; 92: 171–186. doi:10.1016/j.rser.2018.04.095.
25. Richhariya G., Kumar A. Fabrication and characterization of mixed dye: Natural and synthetic organic dye. *Optical Materials*. 2018; 79: 296–301. doi:10.1016/j.optmat.2018.03.056.
26. Higashino T., Iiyama H., Kurumisawa Y., Imahori H. Thiazolocatechol: Electron-withdrawing catechol anchoring group for dye-sensitized solar cells. *ChemPhysChem*. 2019; 20: 2689–2695. doi:10.1002/cphc.201900342.
27. Adineh M., Tahay P., Ameri M., Safari N., Mohajerani E. Fabrication and analysis of dye-sensitized solar cells (DSSCs) using porphyrin dyes with catechol anchoring groups. *RSC Adv*. 2016; 6: 14512–14521. doi:10.1039/C5RA23584G.
28. Krawczyk S., Nawrocka A., Zdyb A. Charge-transfer excited state in pyrene-1-carboxylic acids adsorbed on titanium dioxide nanoparticles. *Spectrochimica Acta Part A: Molecular and Biomolecular Spectroscopy*. 2018; 198: 19–26. doi:https://doi.org/10.1016/j.saa.2018.02.061
29. Krawczak E., Zdyb A. The influence of the dye adsorption time on the DSSC performance. *Kaźmierczak B, Jadwiszczak P, Kutylowska M, Miller U, editors. E3S Web Conf*. 2019; 100: 00040. doi:10.1051/e3sconf/201910000040.
30. Ito S., Chen P., Comte P., Nazeeruddin M.K., Liska P., Péchy P., et al. Fabrication of screen-printing pastes from TiO₂ powders for dye-sensitized solar cells. *Progress in Photovoltaics: Research and Applications*. 2007; 15: 603–612. doi:10.1002/pp.768.
31. Berni A., Mennig M., Schmidt H. Doctor Blade. In: *Aegerter MA, Mennig M, editors. Sol-gel technologies for glass producers and users*. Boston, MA: Springer US; 2004; 89–92. doi:10.1007/978-0-387-88953-5_10.
32. Grätzel M. Recent Advances in sensitized mesoscopic solar cells. *Acc Chem Res*. 2009; 42: 1788–1798. doi:10.1021/ar900141y.
33. Wang Y., Hang K., Anderson N.A., Lian T. Comparison of electron transfer dynamics in molecule-to-nanoparticle and intramolecular charge transfer complexes. *J Phys Chem B*. 2003; 107: 9434–9440. doi:10.1021/jp034935o.
34. Pinto A.L., Cruz L., Gomes V., Cruz H., Calogero G., de Freitas V., et al. Catechol versus carboxyl linkage impact on DSSC performance of synthetic pyranoflavylum salts. *Dyes and Pigments*. 2019; 170: 107577. doi:10.1016/j.dyepig.2019.107577
35. Zdyb A., Krawczak E. Organic Dyes in Dye-Sensitized Solar Cells Featuring Back Reflector. *Energies*. 2021; 14: 5529. doi:10.3390/en14175529